THE INFLUENCE OF CLOUD PROCESSES ON THE DISTRIBUTION OF CHEMICAL SPECIES FOR THE 10 JULY 1996 STERAO/DEEP CONVECTION STORM

Mary C. Barth[1], William C. Skamarock[1], and Amy L. Stuart[2]

[1]National Center for Atmospheric Research, Boulder, Colorado, USA
[2]Stanford University, Stanford, California USA

1. INTRODUCTION

Clouds are able to modify the distribution of chemical species in many ways. Through air motions associated with clouds, chemical species are transported from the boundary layer to the free troposphere. Highly soluble species may dissolve into the cloud water and rain and ultimately be deposited on the ground in the precipitation. Because of the interaction of the cloud hydrometeors, chemical species may be captured by the precipitating ice particles. Photolysis rates are altered by the scattering and attenuation of solar radiation. The cloud hydrometeors may serve as locations for aqueous and ice-phase reactions.

Deep convection is usually thought to transport insoluble chemical species from the boundary layer to the upper troposphere and to rain out highly soluble species. By using a non-hydrostatic, three-dimensional convective cloud model coupled to a simple chemical reaction mechanism, we examine the importance of aqueous chemistry, microphysical processes, and modified photolysis rates compared to transport on the spatial distribution of peroxide species (H_2O_2 and CH_3OOH).

2. MODEL DESCRIPTION

The cloud model used for the simulations is the three-dimensional, fully-compressible, non-hydrostatic COllaborative Model for Multiscale Atmospheric Simulation (COMMAS), which is derived from the Wicker and Wilhelmson (1995) model. This model uses a Van-Leer type, monotonic advective scheme (Wicker and Wilhelmson, 1995) to transport water vapor, cloud water, rain, cloud ice, snow, graupel or hail, and scalars. A second order Runge-Kutta time integration (Wicker and Skamarock, 1998) is used to advance the quantities in time. The ice microphysics parameterization is that described by Tao et al. (1993). For the simulations performed here, hail hydrometeor characteristics ($\rho_h = 0.9$ g cm^{-3}, $N_o = 4 \times 10^4$ m^{-4}) are used.

The model is configured to a 120 x 120 x 20 km domain with 121 grid points in each horizontal direction (1 km resolution) and 51 grid points in the vertical direction with a variable resolution beginning at 50 m at the surface and stretching to 750 m at the top of the domain. A description of the meteorological scenario and transport of passive tracers is found in Skamarock et al. (2000) for the 10 July 1996 STERAO storm. We initialize the model environment and the initiation of convection in the same manner as Skamarock et al..

The gas chemistry (Table 1) represents daytime chemistry of 15 chemical species. The aqueous chemistry (Table 1) is computed for the cloud water and rain assuming a pH of 4.5. This chemistry includes two photolysis reactions whose rates are 1.25 times the interstitial photolysis frequency (S. Madronich, 1996, personal communication). Most chemical species are initialized with values measured in the inflow region of the storm; other species are estimated from values found in the literature or from the July monthly-mean mixing ratio for northeastern Colorado calculated by the 3-dimensional global transport model, MOZART (Brasseur et al., 1998). The initial profile for H_2O_2 and CH_3OOH are noted in Figures 2 and 3.

The chemical mechanism is solved with an Euler backward iterative approximation using a Gauss-Seidel method with variable iterations. A convergence criterion of 0.01% is used for all the species.

3. RESULTS

In general, the simulated storm reproduces the structure and dynamics of the observed storm (Skamarock et al., 2000). Both the observed and simulated storm evolve from a multicellular convective system to a supercellular system. Here, results after 1 hour of integration are discussed. These results reflect the multicellular stage of the storm when there are three updraft cores. Previous simulations indicate that 75% of the air parcels had a residence time between 500 and 1200 seconds traveling from 4 km m.s.l. to 500 meters below the air parcel's maximum attained height in the updraft (Skamarock et al., 2000), and that 74% of the air parcels had a residence time in contact with liquid water between 400 and 800 seconds (Barth et al., 2000). This short residence time in contact with liquid water may limit the influence the liquid water has on the chemical species (via aqueous chemistry, separation of soluble and insoluble species, or washout).

Corresponding author address: Mary C. Barth, NCAR, P.O. Box 3000, Boulder, CO 80307-3000. Email: barthm@ucar.edu

Table 1. Chemical reactions depicted in chemistry module.

		k_{298}	$\frac{E}{R}$
	Gas-Phase Reactions		
O_3 + hν	$\rightarrow$ 2 OH	3.41×10^{-6}	
NO_2+ hν	$\rightarrow$ NO + O_3	3.65×10^{-3}	
H_2O_2 + hν	$\rightarrow$ 2OH	2.19×10^{-6}	
CH_2O+ hν+ $2O_2$	$\rightarrow$ $2HO_2$ + CO	7.84×10^{-6}	
CH_2O+ hν	$\rightarrow$ H_2+ CO	1.48×10^{-5}	
CH_3OOH+ hν+ O_2	$\rightarrow$ CH_2O+ HO_2 + OH	1.66×10^{-6}	
HNO_3 + hν	$\rightarrow$ NO_2+ OH	1.25×10^{-7}	
O_3 + NO	$\rightarrow$ NO_2+ O_2	1.8×10^{-14}	1400.
O_3 + OH	$\rightarrow$ HO_2 + O_2	6.8×10^{-14}	940.
O_3 + HO_2	$\rightarrow$ OH + $2O_2$	2.0×10^{-15}	
NO_2+ OH + M	$\rightarrow$ HNO_3 + M	$k_o=2.6\times10^{-30}(\frac{T}{300})^{-3.2}$	
		$k_\infty=2.4\times10^{-11}(\frac{T}{300})^{-1.3}$	
H_2O_2 + OH	$\rightarrow$ HO_2 + H_2O	1.7×10^{-12}	160.
HO_2 + HO_2	$\rightarrow$ H_2O_2 + O_2	2.9×10^{-12}	-590.
HO_2 + OH	$\rightarrow$ H_2O+ O_2	1.1×10^{-10}	-250.
OH + OH	$\rightarrow$ O_3 + H_2O	1.9×10^{-12}	240.
OH + OH + M	$\rightarrow$ H_2O_2 + M	$k_o=6.9\times10^{-31}(\frac{T}{300})^{-0.8}$	
		$k_\infty=1.5\times10^{-11}$	
HO_2 + NO	$\rightarrow$ NO_2+ OH	8.6×10^{-12}	-250.
HNO_3 + OH	$\rightarrow$ $0.89NO_2$+ $0.89O_3$ + 0.11 NO	1.0×10^{-13}	-785.
CH_4 + OH + O_2+ M	$\rightarrow$ CH_3OO+ H_2O+ M	6.3×10^{-15}	1800.
CH_3OO+ NO + O_2	$\rightarrow$ CH_2O+ HO_2 + NO_2	7.7×10^{-12}	-180.
CH_3OO+ HO_2	$\rightarrow$ CH_3OOH+ O_2	5.6×10^{-12}	-800.
CH_3OO+ CH_3OO	$\rightarrow$ $1.4CH_2O$+ $0.8HO_2$ + 0.6HCOOH	4.7×10^{-13}	-190.
CH_2O+ OH + O_2	$\rightarrow$ CO + H_2O+ HO_2	1.0×10^{-11}	
CH_3OOH+ OH	$\rightarrow$ $0.7CH_3OO$+ $0.3CH_2O$+ 0.3 OH + H_2O	7.4×10^{-12}	-200.
CO + OH + O_2	$\rightarrow$ CO_2 + HO_2	2.4×10^{-13}	
HCOOH+ OH + O_2	$\rightarrow$ HO_2 + CO_2 + H_2O	3.2×10^{-13}	
SO_2 + OH + M	$\rightarrow$ $SO_4^=$	$k_o=3.0\times10^{-31}(\frac{T}{300})^{-3.3}$	
		$k_\infty=1.5\times10^{-12}$	
	Aqueous-Phase Reactions		
O_3 + hν+ H_2O	$\rightarrow$ H_2O_2 + O_2	4.26×10^{-6}	
H_2O_2 + hν	$\rightarrow$ 2OH	2.73×10^{-6}	
H_2O_2 + OH	$\rightarrow$ HO_2 + H_2O	2.7×10^{7}	1700.
HO_2 + O_2^-	$\rightarrow$ HO_2^-+ O_2	1.0×10^{8}	1500.
OH + HO_2	$\rightarrow$ H_2O+ O_2	1.0×10^{10}	1500.
O_3 + O_2^-+ H_2O	$\rightarrow$ OH + $2O_2$+ OH^-	1.5×10^{9}	1500.
CH_3OO+ O_2^-+ H_2O	$\rightarrow$ CH_3OOH+ OH^-+ O_2	5.0×10^{7}	1600.
CH_3OOH+ OH	$\rightarrow$ CH_3OO+ H_2O	2.7×10^{7}	1700.
CH_3OOH+ OH	$\rightarrow$ $CH_2(OH)_2$+ OH	1.9×10^{7}	1900.
$CH_2(OH)_2$+ OH + O_2	$\rightarrow$ HCOOH+ HO_2 + H_2O	2.0×10^{9}	1510.
HCOOH+ OH + O_2	$\rightarrow$ CO_2 + HO_2 + H_2O	1.6×10^{8}	1510.
$HCOO^-$+ OH + O_2	$\rightarrow$ CO_2 + HO_2 + OH^-	2.5×10^{9}	1510.
HSO_3^- + H_2O_2 + H^+	$\rightarrow$ $SO_4^=$+ $2H^+$+ H_2O	$\frac{4.0\times10^{7}[H^+]}{1.+13[H^+]}$	4800.
HSO_3^- + O_3	$\rightarrow$ $SO_4^=$+ H^++ H_2O	3.7×10^{5}	5530.
$SO_3^=$+ O_3	$\rightarrow$ $SO_4^=$+ O_2	1.5×10^{9}	5280.

Reaction rates are of the form $k = k_{298}\exp[-\frac{E}{R}(\frac{1}{T} - \frac{1}{298})]$ unless otherwise noted. Units for first order reactions are s^{-1}, second order gas reactions cm^3 s^{-1}, and second order aqueous reactions M^{-1} s^{-1}.

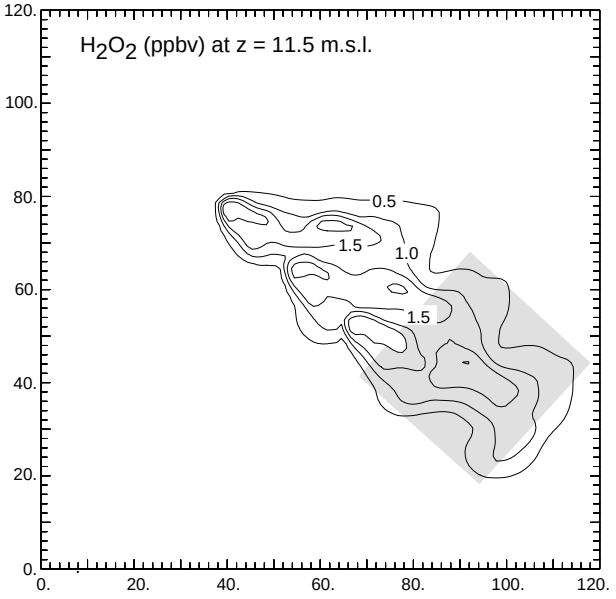

Figure 1. Passively transported H_2O_2 mixing ratio at z = 11.5 km m.s.l. and t = 3600 s.

The anvil, which had a northwest-southeast orientation, is composed primarily of snow and ice. Figure 1 shows a non-reactive H_2O_2 mixing ratio (i.e., the tracer is initialized with the H_2O_2 profile in Figure 2, but is merely transported during the simulation) at an altitude of 11.5 km (middle of the anvil). The multicellular nature of the storm is evident with mixing ratios of 2 ppbv reaching the anvil. The outflow region, marked in Figure 1 by the gray box, is analyzed to examine the effect aqueous chemistry and ice hydrometeors have on the peroxide species. Figures 2 and 3 show the average mixing ratio of H_2O_2 and CH_3OOH for the outflow region marked by the gray box in Figure 1. Besides the initial profile, results of 4 simulations are shown.

3.1 Transport

The transport-only simulation initializes all of the chemical species with their initial mixing ratios, but does not allow any chemistry or dissolution of the species. The species are only transported. Compared to the initial profile H_2O_2 was transported from below 6 km m.s.l. to the region above 6 km m.s.l. and below 15 km m.s.l. CH_3OOH shows similar transport, except the region above 8 km m.s.l. and below 11 km m.s.l. where CH_3OOH is removed via transport.

3.2 Gas Chemistry

The gas chemistry only simulation transports the chemical species and calculates gas chemistry (no aqueous chemistry and no dissolution into liquid hydrometeors). Compared to the transport-only profile, H_2O_2 mixing ratios from the gas chemistry only simulation are generally higher above 6 km m.s.l., and are similar in value above 11 km m.s.l. CH_3OOH also shows this trend, indicating that the peroxy radicals, which produce the peroxides, are greater between 6 and 11 km m.s.l.

3.3 Aqueous Chemistry

The gas and aqueous chemistry simulation transports the chemical species, calculates gas and aqueous chemistry, but does not allow the ice to capture the dissolved chemical species. When riming occurs, it is assumed in this simulation that the dissolved chemical species degasses from the cloud water or rain. Compared to the gas-only profile, H_2O_2 mixing ratios from the gas and aqueous chemistry simulation is very similar. This is also the case for CH_3OOH. It is surprising that H_2O_2 does not show greater depletion due to aqueous chemistry, especially since SO_2 has mixing ratios of about 1 ppbv in the boundary layer. We could speculate that H_2O_2 is being produced in the aqueous phase (photolysis of O_3 and/or reaction of peroxy radical with superoxide), but SO_2 mixing ratios averaged in the area of the outflow of the storm are not depleted. Without a more detailed analysis, we can only assume that the short residence time in contact with liquid water (less than 800 seconds) is not sufficiently long enough to allow aqueous chemistry to proceed.

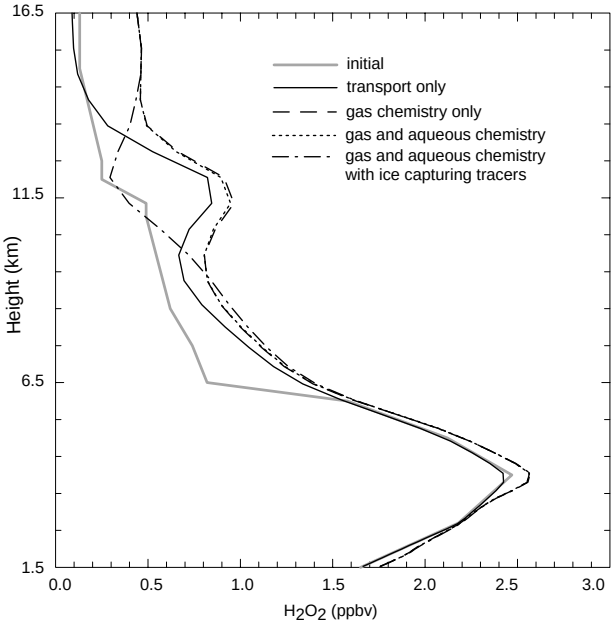

Figure 2. Average vertical profiles of H_2O_2 mixing ratio for the passively transported, gas chemistry only, gas and aqueous chemistry with degassing when freezing occurs, and gas and aqueous chemistry with capture when freezing occurs at t = 3600 s in an area demarked by the gray box illustrated in Figure 1.

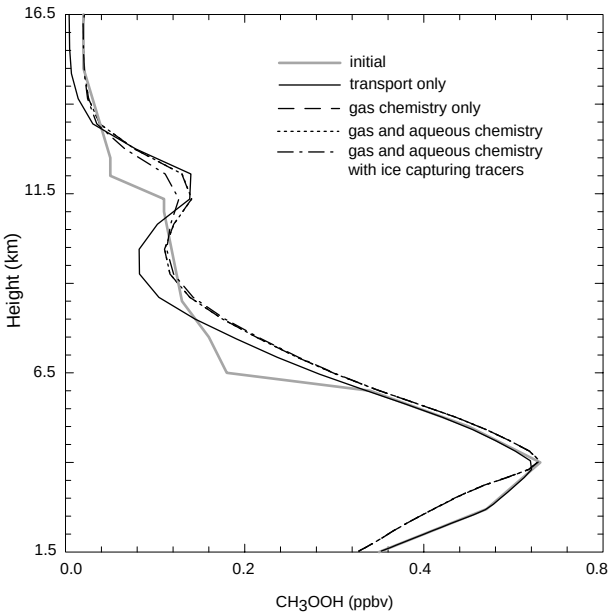

Figure 3. Same as Figure 2 except for CH_3OOH.

3.4 Microphysical Processes

The gas and aqueous chemistry with ice capturing tracers simulation transports the chemical species, calculates gas and aqueous chemistry, and allows the ice to capture the dissolved chemical species. When riming occurs, it is assumed in this simulation that the frozen hydrometeor retains the chemical species and the chemical species moves with the frozen hydrometeor allowing it to precipitate. Compared to the gas and aqueous chemistry profile, H_2O_2 is substantially depleted in the outflow of the convection (10 to 14 km m.s.l.). CH_3OOH is also depleted, but not as much as H_2O_2. At z = 11.5 km m.s.l., H_2O_2 is depleted by 55-60% whereas CH_3OOH is depleted by 14%. These results are similar to those found by Barth et al (2000) for soluble tracers. Barth et al noted a 35% depletion for a tracer with a solubility similar to H_2O_2 and no depletion for a tracer with a solubility similar to CH_3OOH. Differences between these numbers may be due to this study allowing the solubility of the species to vary with temperature (solubility increases as temperature decreases) or may be due to the gas and aqueous chemistry that occur in this study.

4. DISCUSSION

4.1 Scavenging Efficiency

Cohan et al (1999) determined the scavenging efficiency of soluble species from measurements of soluble and insoluble species obtained in the boundary layer, the convectively-influenced upper troposphere, and the upper troposphere unaffected by convection. They found that H_2O_2 has a scavenging efficiency of 55-70%. If we do the same calculation here for the simulation where gas and aqueous chemistry were predicted as well as transport and capture of the dissolved species by frozen hydrometeors, we find that H_2O_2 has a scavenging efficiency of 74% and CH_3OOH has a scavenging efficiency of 14%. These values can have quite a large uncertainty because both peroxides have a strong gradient in mixing ratio in the boundary layer.

4.2 Effect of the Cloud on Photolysis Rates

The influence of the storm upon photolysis rates has not yet been assessed, but we speculate that higher mixing ratios of H_2O_2 would be found in brighter regions of the storm (to the west and top) because hydroxyl and peroxy radicals would be enhanced in these regions.

5. ACKNOWLEDGMENTS

The National Center for Atmospheric Research is sponsored by the National Science Foundation. X.X. Tie is thanked for providing output for northeastern Colorado from the 3-d global chemistry transport model.

6. REFERENCES

Barth, M. C., A. L. Stuart, and W. C. Skamarock, 2000: The fate of soluble tracers in deep convection, in preparation.

Brasseur, G. P., D. A. Hauglustaine, S. Walters, P. J. Rasch, J.-F. Müller, C. Granier, and X. X. Tie, 1998: MOZART: A global chemical transport model for ozone and related chemical tracers, Part 1. Model Description, *J. Geophys. Res.*, **103**, 28,265-28,289.

Cohan, D. S., Schultz, M. G., Jacob, D. J., Heikes, B. G., and Blake, D. R., 1999: Convective injection and photochemical decay of peroxides in the tropical upper troposphere: methyl iodide as a tracer of marine convection, *J. Geophys. Res.*, **104**, 5717-5724.

Skamarock, W. C., J. Powers, M. C. Barth, J. E. Dye, T. Matejka, D. Bartels, K. Baumann, J. Stith, D. D. Parrish, and G. Hubler, 2000: Numerical simulations of the 10 July STERAO/Deep Convection Experiment convective system: Dynamics and transport, *J. Geophys. Res.*, accepted.

Tao, W.-K. and J. Simpson, 1993: Goddard cumulus ensemble model. Part I: Model description, TAO, **4**, 35-72.

Wicker, L. J. and W. C. Skamarock, 1998: A time splitting scheme for the elastic equations incorpo-

rating second-order Runge-Kutta time differencing, *Mon. Wea. Rev.*, , **126**, 1992–1999.

Wicker, L. J. and R. B. Wilhelmson, 1995: Simulation and analysis of tornado development and decay within a three-dimensional supercell thunderstorm, *J. Atmos. Sci.*, **52**, 2675-2703.